water

MDPI

Article

# Effects of Pressure and Nozzle Size on the Spray Characteristics of Low-Pressure Rotating Sprinklers

**Rui Chen, Hong Li *, Jian Wang and Xin Guo**

Research Centre of Fluid Machinery Engineering and Technology, Jiangsu University, Zhenjiang 212013, China; chenruinws@foxmail.com (R.C.); wangjiannsw@163.com (J.W.); guoxin970203@163.com (X.G.)

* Correspondence: hli@ujs.edu.cn; Tel.: +86-511-8879-7658

Received: 29 July 2020; Accepted: 14 October 2020; Published: 17 October 2020

check for updates

**Abstract:** Using low-pressure sprinklers in agricultural irrigation has become an alternative way of reducing water and energy stress. To determine the applicability of the low-pressure rotating sprinkler, an experiment was conducted to evaluate the effects of working pressure and nozzle size on sprinkler rotation speed, application rate, droplet size, droplet velocity, droplet trajectory angle, and kinetic energy distribution. The results showed that the mean droplet diameter increased exponentially along with the increase in distance from the sprinkler, and a logarithmic relation was derived between droplet diameter and droplet velocity. Due to the low breakup degree of the jet under the lowest working pressure of 100 kPa, the peak values of specific power and application rate were high, which reached 0.09 W m$^{-2}$ and 11.35 mm h$^{-1}$, and were 3.1–5.4 times and 2.5–3.1 times those of other working conditions. Meanwhile, the peak specific power of the biggest nozzle (diameter = 5.2 mm) was 2.4–2.8 times that of smaller nozzles. With an increase in working pressure, the sprinkler time per rotation decreased and the distributions of kinetic energy and water became more uniform. Thus, it is not recommended to equip the sprinkler with a large nozzle under low working pressure.

**Keywords:** sprinkler irrigation; application rate; droplet size; kinetic energy; low pressure

## 1. Introduction

Water shortage and the energy crisis continue to be worldwide challenges, especially in the arid regions that cover 42% of the planet's surface [1]. According to UNESCO [2], agricultural irrigation uses 69% of the water utilized by humans. To reduce water consumption in agriculture, water-saving irrigation technologies, including drip irrigation and sprinkler irrigation, have been actively developed and promoted [3]. However, irrigation technology consumes a large amount of energy in practice [4]. Taking these challenges into consideration, many studies have focused on improving the water and energy efficiencies of irrigation systems [5–7].

Sprinkler irrigation is one of the most commonly used agricultural irrigation methods, with 21% of irrigated land in China and 55% of the total irrigated land in the United States being equipped with sprinkler systems [8,9]. Traditional sprinkler irrigation systems were usually designed to operate at a minimum of 300 kPa of pressure at the nozzles of the sprinklers [10]. Compared with the working pressure of the emitter used in drip irrigations (20–100 kPa), the operating pressure of the sprinkler was extremely high [11]. With the aim of reducing energy consumption and improving water use in sprinkler irrigation systems, Jiménez-Bello et al. [12] developed a methodology to minimize energy consumption by grouping intakes of pressurized irrigation networks into sectors. Meanwhile, reductions in the energy requirements of center pivot and lateral-move irrigation machines have successfully been achieved by replacing the traditional impact sprinklers with spray sprinklers [10]. Martínez et al. [13] noted that reducing the operating pressure of the sprinkler and using low-pressure sprinklers can significantly decrease the operating cost. However, most of the studies on low-pressure sprinklers have been confined to fixed spray plate sprinklers (FSPSs) and rotating spray plate sprinklers (RSPSs) [14–16]. Studies conducted with solid-set rotating sprinklers, especially those working under low-pressure (lower than 300 kPa), are uncommon [8], even though solid-set rotating sprinklers have a wide application in agriculture, and are appropriate for sloping farmland and irregular fields [17].

As one of the core components of sprinkler irrigation systems, the sprinklers' spray characteristics may directly affect irrigation performance and system cost. The characteristics of the droplets discharged by a water jet of an agricultural sprinkler have a major influence on evaporation and drift losses, impacting the infiltration capacity of the soil and distorting the water distribution pattern applied by the sprinkler [14,18]. The droplet characteristics primarily include the size, velocity, and kinetic energy, which depend on (1) the type of sprinkler, (2) the nozzle size, and (3) the working pressure [19]. The test technique for droplet characterization has developed from the use of flour pellets, oil immersion, and photographic methods to laser precipitation monitoring and the use of a two-dimensional video disdrometer [14,19]. Meanwhile, ballistic models and the upper limit lognormal distribution model have been used to predict the distribution of droplet sizes [20]. Based on the information about droplet sizes and velocities, the relationships between the droplet size and the working pressure, nozzle size, and distance to the sprinkler were established for different types of sprinklers by the aforementioned researchers. The kinetic energy of sprinkler water, which was determined by droplet characterization, was found to be the key parameter in determining the effects of sprinkler irrigation on soil properties [21]. When the kinetic energy of droplets impacted the soil surface and soil particles were detached, then the overland flow transporting the soil particles was the main process causing soil erosion [22,23]. Moreover, crust formation attributed to droplet impact was a problem for the emergence of the seedlings of crops such as sugar beets [24]. The previous studies played an important role in the development of sprinklers and the design of sprinkler irrigation systems. However, most of the studies focused on standard-pressure sprinklers [19,20] and spray plate sprinklers [14,15,21], but rarely for low-pressure rotating sprinklers used in solid-set irrigation systems. Due to the low degree of jet flow breakup under low working pressures, runoff was the largest potential water loss for low-pressure sprinkler irrigation systems [25].

The low-pressure rotating sprinkler was designed for use in solid-set sprinkler irrigation systems and can potentially achieve a high quality of water application under a low working pressure if the structure is properly designed. Zhang et al. [8] assessed whole-field sprinkler irrigation application uniformity of low-pressure and standard-pressure rotating sprinklers, but the droplet characteristics and kinetic energy distribution were not investigated. Due to the difficulty in measurement created by the discrete water streams emitted, research on the kinetic energy of sprinklers has been limited. Since the kinetic energy has a major influence on runoff and soil erosion from sprinkler irrigation [21], the effects of nozzle size and working pressure and their interaction on the kinetic energy and droplet characteristics of the sprinkler should be further studied. A comprehensive evaluation of the spray characteristics for the low-pressure rotating sprinkler is especially needed since this can help to avoid centralized distribution of kinetic energy due to low working pressure, while also lowering the system energy consumption by reducing the operating pressure reasonably. However, information on low-pressure rotating sprinklers provided by the manufactures is restricted to basic parameters such as available operating pressure ranges and flow rates [26], which does not offer information related to the kinetic energy and droplet size distribution.

Based on the above-mentioned considerations, the objective of this study was to determine the spray characteristics of a low-pressure rotating sprinkler. The rotation speed, distribution of water application, droplet size, velocity, and kinetic energy of the sprinkler were investigated. It also aimed to discover if these characteristics are affected by different factors, such as the working pressure and nozzle size. These results will be used to provide guidance for the development of low-pressure sprinklers and will also be helpful in improving the use of water for field irrigation by low-pressure sprinkler irrigation systems.

## 2. Materials and Methods

### 2.1. Sprinkler

A low-pressure rotating sprinkler (Nelson R33LP; Nelson Irrigation Co., Walla Walla, WA, USA) with three nozzle diameters of 4.4, 4.8, and 5.2 mm was used in the experiments. Figure 1 illustrates the components of the sprinkler. In order to determine the droplet characteristics under low working pressure, the operating pressure used in this study ranged from 100 to 300 kPa in intervals of 50 kPa, and the minimum working pressure was lower than the working pressure recommended by the manufacturer (175–350 kPa).

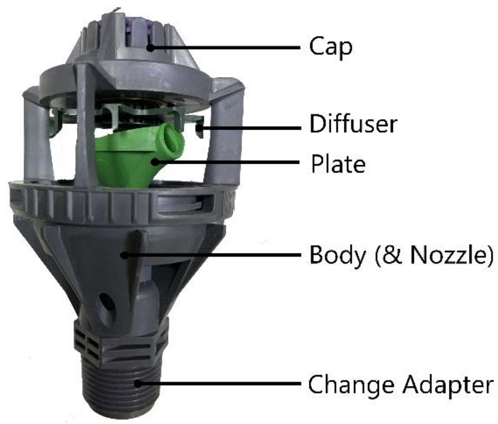


**Figure 1.** Components of the low-pressure rotating sprinkler.

### 2.2. Experimental Setup and Procedure

The indoor experiments designed to evaluate the droplet characteristics of the low-pressure rotating sprinkler were performed at the Irrigation Laboratory of the Research Centre of Fluid Machinery Engineering and Technology (Jiangsu University, Zhenjiang City, Jiangsu Province, P.R. China). The design of the experimental setup was in accordance with the ISO 15886-3 and ASAE S398.1 standards [27,28]. Figure 2 includes a photograph and schematic of the experiment. Water was supplied from a constant-level reservoir by a frequency pump (5 $m^3$ $h^{-1}$, 580 kPa). The discharge flow rate of the sprinkler was measured by an electromagnetic flow meter with an accuracy tolerance of 0.5%. The sprinkler was installed 1.5 m above the ground level, and an Asmik MIK-Y190 model pressure gauge (0–600 kPa, accuracy 0.4%) was placed 0.1 m under the nozzle. A pressure valve was attached to control the water head at the inlet of the sprinkler.

The catch cans for determining the water application data were plastic containers with a 20-cm opening diameter and 54-cm height. The catch cans were placed on a level surface along two radii, which were determined by two lines extending from the sprinkler at a 90° angle. On the radii, the catch cans were spaced at 1-m intervals, with a 0.5-m radial increment used at the end of the wetted radius when necessary (Figure 2b). The end of each line of the catch cans was extended beyond the wetted area of the sprinkler for each combination of operating pressure and nozzle size in this study. The test time for determining the water distribution was 1 h, and the depth of water from each catch can was recorded immediately after each test [29]. The radial water application data were averaged for the water depth for the two radii of catch cans.

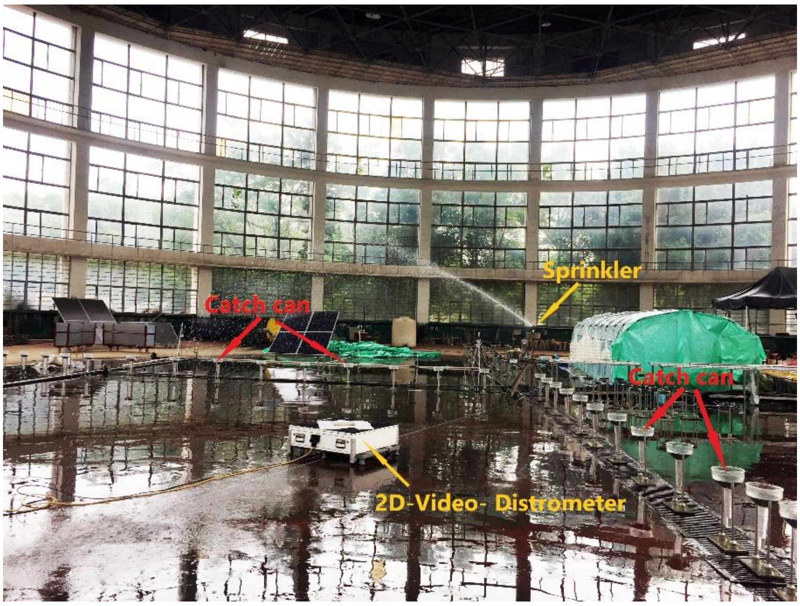


(**a**)

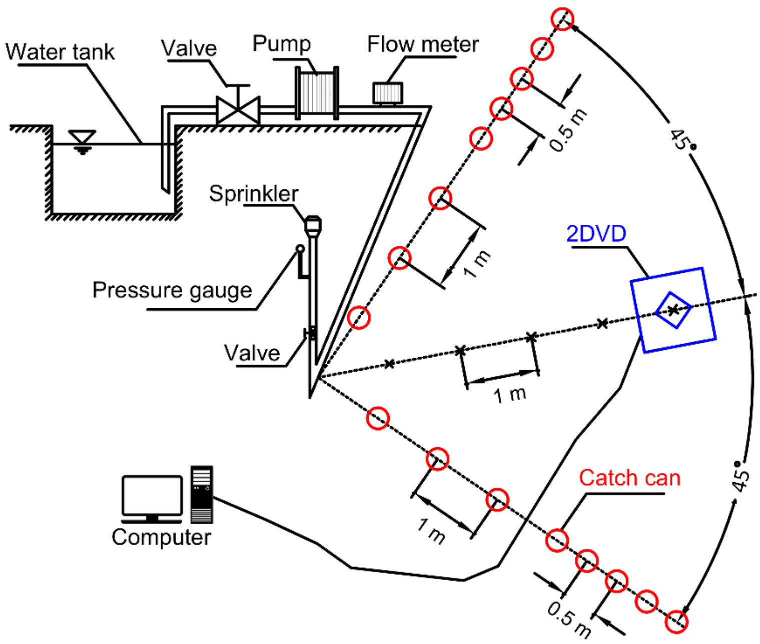


(**b**)

**Figure 2.** View inside the laboratory test facility: (**a**) photo; and (**b**) schematic.

A two-dimensional video disdrometer (2DVD) (Joanneum Research Co., Graz, Styria, Austria) was used to measure the droplet size and velocity (Figure 2). As shown in Figure 3, two vertically disposed CCD cameras inside the instrument made linear scans of droplets passing through the test area and recorded the individual droplet size and the vertical and horizontal velocity components [26,30]. The measurement area of the 2DVD was 100 mm × 100 mm (Figure 3b), and its total height was 33 cm. The droplet size measurement principle of the 2DVD is illustrated in Figure 4; as water droplets passed through the test area, the widths of their shadows were scanned and recorded by the cameras, and the shadow widths were used to reconstruct each droplet's shape in two dimensions. The two-dimensional shape of each droplet as determined by the two cameras was then used to reconstruct the three-dimensional shape of the droplet, and the droplet volume was also estimated. The droplet diameter was calculated using the equal volume of the sphere.

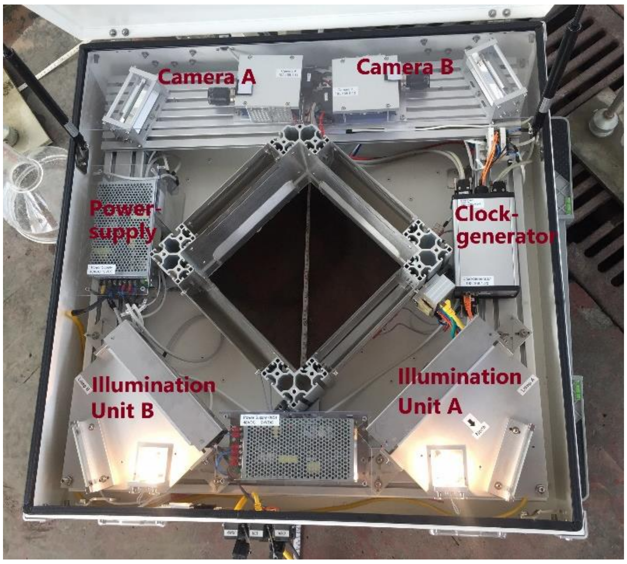


(**a**) 2DVD

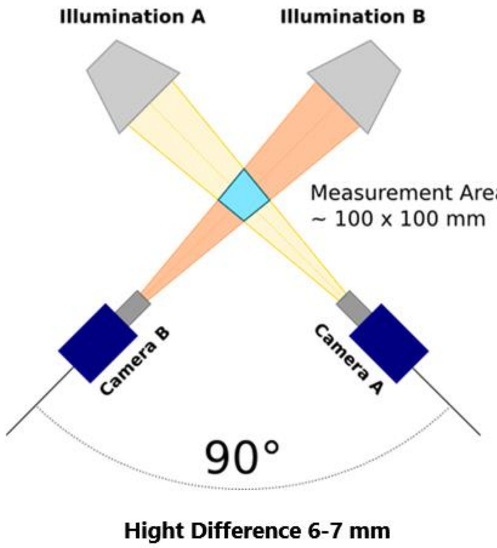


(**b**) Testing area of the 2DVD

**Figure 3.** Two-dimensional video disdrometer (2DVD) (**a**) and testing area of the 2DVD (**b**).

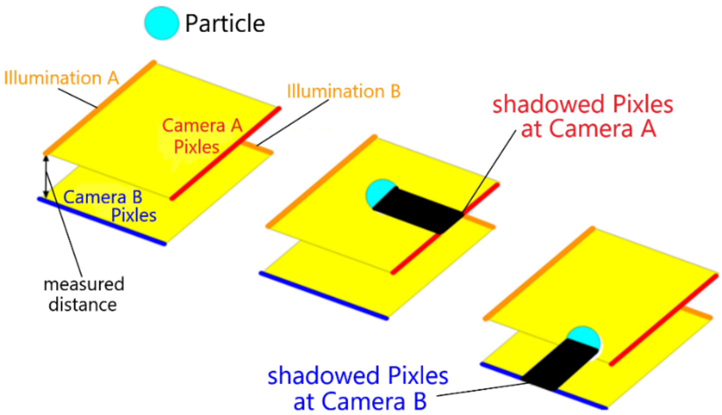


**Figure 4.** Principle of droplet size measurement.

The water droplet velocity was determined by measuring the time required for the droplet to pass the two cameras (Figure 5). The measured velocity of an individual water droplet includes the vertical velocity and the horizontal velocity. The vertical velocity of a water droplet was calculated by Equation (1). The horizontal velocity of a water droplet was composed of the two-horizontal velocities of the droplet passing camera A and camera B, and the droplet horizontal velocity was calculated by Equation (2). The combined velocity of a water droplet was determined by the vertical velocity and the horizontal velocity, which was calculated using Equation (3).

$$v_v = {}^{2H}/_{(t_2 - t_0) + (t_3 - t_1)} \tag{1}$$

$$v_h = \sqrt{{v_a}^2 + {v_b}^2} = \sqrt{\left(\frac{L_a}{t_1 - t_0}\right)^2 + \left(\frac{L_b}{t_3 - t_2}\right)^2} \tag{2}$$

$$v_c = \sqrt{{v_v}^2 + {v_h}^2} \tag{3}$$

where $v_v$ is the vertical velocity of the droplet in m s$^{-1}$; $v_h$ is the horizontal velocity of the droplet in m s$^{-1}$; $v_c$ is the combined velocity of the droplet in m s$^{-1}$.

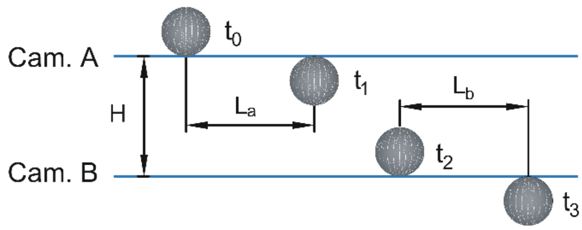


**Figure 5.** Principle of droplet velocity measurement.

In the radial test of kinetic energy distribution, the testing locations for the 2DVD was set at 1-m increments from the sprinkler along the spraying direction (Figure 2b). The duration of measurements at each radial location was at least 5 min, ensuring that the number of water droplets collected at each testing location was more than 5000.

The sprinkler time per rotation was measured using a stopwatch. The duration of measurements for each combination of nozzle size and working pressure was at least 10 min, and the number of turns of sprinkler rotation and the test time was recorded. The average rotation speed was used as the final experimental data.

## 2.3. Data Analysis

### 2.3.1. Droplet Size and Drop Velocity

The size distribution of the droplets discharged by the water jet of a sprinkler is important, as this can explain several processes related to water distribution [14]. In this study, the diameters of the measured water droplets ranged from 0.1 to 8.94 mm. The volume-weighted mean particle size (VMD) of droplets was adopted in this study and was calculated using Equation (4). For a given droplet diameter, the arithmetic mean velocity of droplets was calculated using Equation (5).

$$d_V = \frac{\sum_{i=1}^{n} {d_i}^4}{\sum_{i=1}^{n} {d_i}^3} \tag{4}$$

$$\bar{v}_d = \frac{\sum_{j=1}^{m} v_j}{m} \tag{5}$$

where $d_V$ is the droplet VMD in mm; $d_i$ is the diameter of the $i$-th droplet in mm; $n$ is the number of droplets; $\bar{v}_d$ is the mean velocity of a droplet of $d$-mm diameter in m s$^{-1}$; $v_j$ is the velocity of the $j$-th droplet in m s$^{-1}$; $m$ is the number of droplets of $d$-mm diameter.

### 2.3.2. Droplet Angle

The trajectory angle when the droplet impacts the ground is an important index of sprinkler spray characteristics. The shear rate of the droplet creates a shear stress on the soil surface, which causes the detachment of soil particles from the soil surface and the transport of these soil particles, leading to soil erosion [31]. The droplet trajectory angle refers to the angle between the droplet's landing direction and the horizontal ground. The mean droplet trajectory angle $A_{di}$ (°) at the $i$-th radial location was calculated using Equation (6).

$$A_{di} = \frac{\sum_{j=1}^{Nd_i} arcsin\, {v_{vj}}/{v_{cj}}}{Nd_i} \tag{6}$$

where $Nd_i$ is the number of droplets measured at the $i$-th radial location; $v_{vj}$ is the vertical velocity of the $j$-th droplet in m s$^{-1}$; $v_{cj}$ is the combined velocity of the $j$-th droplet in m s$^{-1}$.

2.3.3. Kinetic Energy

The kinetic energy ($E_{sd}$) of a single droplet was calculated using Equation (7):

$$E_{sd} = \frac{1}{12}\pi \times \rho_w \times d^3 \times {v_d}^2 \tag{7}$$

where $E_{sd}$ is the kinetic energy of the single droplet in J; $\rho_w$ is the mass density of water in kg m$^{-3}$; $d$ is the droplet diameter in m; $v_d$ is the velocity of the droplet with a diameter of $d$ m in m s$^{-1}$.

The kinetic energy per unit sprinkler discharge, $KE_{di}$ (J L$^{-1}$), at the $i$-th radial location for each sprinkler was calculated using Equation (8) [31,32].

$$KE_{di} = \frac{\sum_{j=1}^{Nd_i} E_{sd}}{1000 \sum_{j=1}^{Nd_i} \frac{\pi {d_j}^3}{6}} \tag{8}$$

where $Nd_i$ is the number of droplets measured at the $i$-th radial location; $d_j$ is the measured diameter of the $j$-th droplet in m. The resulting value represents the average kinetic energy per liter of droplet volume applied at the $i$-th radial measurement location.

The specific power ($SP$ in W m$^{-2}$), at the $i$-th radial location was computed for each sprinkler using Equation (9) [31,32].

$$SP_i = KE_{di} \times \frac{AR_i}{3600} \tag{9}$$

where $AR_i$ is the application rate associated with the $i$-th radial location in mm h$^{-1}$. Specific power represents the rate at which kinetic energy is transferred to the soil surface.

2.3.4. Performance function

The performance of proposed empirical equations for predicting the various variables were evaluated using the Root Mean Squared Error (RMSE) as presented in Equation (10):

$$RMSE = \sqrt{\frac{1}{n}\sum_{i=1}^{n}\left(y_{mea,i} - y_{cal,i}\right)^2} \tag{10}$$

where $n$ is the measurement time; $y_{mea,i}$ is the VMD through measurement in mm; $y_{cal,i}$ is the VMD through the calculation in mm.

## 3. Results and Analysis

### *3.1. Sprinkler Rotation*

The sprinkler rotation speed is one of the variables that influence the sprinkler spray characteristics. Table 1 gives the sprinkler time per rotation of the three nozzles under five different working pressures. It can be seen that the sprinkler rotation time decreased with increasing working pressure. Nonlinear regression analysis was conducted to examine the effects of the working pressure and nozzle size on the sprinkler rotation speed. The results demonstrate that working pressures have a significant influence on the rotation speed of the low-pressure rotating sprinkler ($p < 0.01$), while the sprinkler rotation speed was not affected by the nozzle size ($p = 0.77$). This result is not in accordance with the rotation of the RSPS reported by Liu et al., who found that the rotation time of the RSPS decreases with increasing nozzle size [33]. As the functioning principles of the R33LP and RSPS are different, the R33LP sprinkler has a more complex structure than that of the RSPS, the damping parts of the R33LP may also have a greater influence on the sprinkler rotation time.

**Table 1.** Sprinkler rotation time under different working pressures.

| Rotation Time (s/Rotation) | | | | | |
|---|---|---|---|---|---|
| Nozzle Size (mm) | Working Pressure (kPa) | | | | |
| | 100 | 150 | 200 | 250 | 300 |
| 4.4 | 184.86 | 97.50 | 64.57 | 47.23 | 38.27 |
| 4.8 | 113.25 | 73.09 | 51.80 | 39.65 | 30.94 |
| 5.2 | 162.86 | 92.14 | 58.62 | 41.08 | 30.80 |

### *3.2. Radial Water Application Rate*

The radial water application rate of the sprinkler with the three nozzle sizes under different working pressures is represented in Figure 6. The radial application rate of the sprinkler presented a unimodal distribution under the lowest working pressure of 100 kPa. The peak values of application rate at the lowest working pressure of 100 kPa were 8.51, 7.28, and 11.35 mm $h^{-1}$ for nozzle sizes of 4.4, 4.8, and 5.2 mm, respectively. That was because when the working pressure was low, the breakup degree of the jet flow released from the sprinkler was low, leading to an insufficient diffusion of water along the radial direction, which easily formed a high peak value of the application rate. As the working pressure increased, the peak value of the application rate decreased, and the radial water distribution of the sprinkler became more uniform. At a given working pressure, the application rate of the sprinkler increased with an increase in the nozzle size (Figure 6). Taking the working pressure of 250 kPa as an example, the average application rates of the sprinkler were 1.97, 2.17, and 2.64 mm $h^{-1}$ at the nozzle diameters of 4.4, 4.8, and 5.2 mm, respectively. In addition, it can be seen from Figure 6 that the wetted radius of the sprinkler increased with the increases in working pressure and nozzle size.

As shown in Figure 6, the error bars for the application rate for all nozzle sizes were largest under the lowest working pressure of 100 kPa, which illustrates a non-uniform water distribution in a circular direction. This can be explained because under the lowest pressure of 100 kPa, the impact force from the nozzle to the plate was not sufficiently large to overcome its resistance, and an unstable rotation was observed, which made the rotation speed randomly decrease; hence, the error bars became large. Therefore, the difference in peak error values for the three nozzles can be attributed to the different rotation speeds of the nozzles. At the lowest working pressure of 100 kPa, the peak error values for the application rate were 3.49, 1.08, and 2.17, and the sprinkler times per rotation were 184.86, 113.25, and 162.86 s (Table 1) for the nozzle sizes of 4.4, 4.8, and 5.2 mm, respectively. With an increase in working pressure, the impact force increased, the rotation speed of the sprinkler increased, and the error bars became small. Consequently, the rotation speed of the sprinkler influenced spray uniformity. If the rotation speed is unstable, the water distribution of the sprinkler is non-uniform in the circular direction.

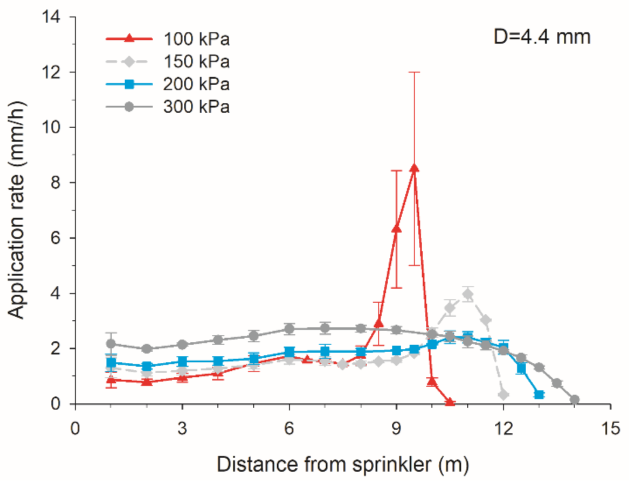


(**a**)

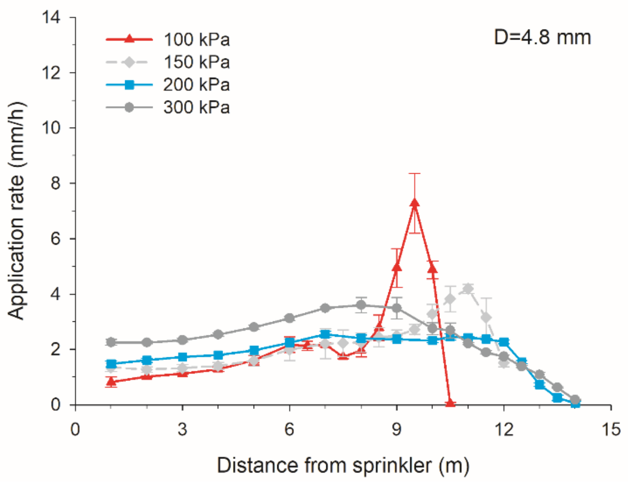


(**b**)

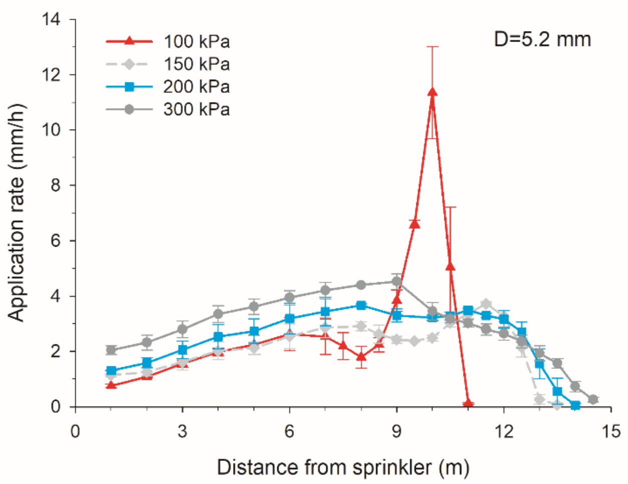


(**c**)

**Figure 6.** Radial application rate under different working pressures. (**a**) D = 4.4 mm, (**b**) D = 4.8 mm, (**c**) D = 5.2 mm.

## *3.3. Droplet Size*

The VMDs of the sprinkler under different operating pressures are shown in Figure 7. The droplet diameter increased exponentially with distance from the sprinkler, in accordance with the previous studies [14,19,34]. However, the sprinklers of interest in these studies were impact sprinklers and FSPSs. As seen in Figure 7, the droplet VMD values at the same distance from the sprinkler decreased with increasing working pressures, which verified the conclusion of Montero et al. [35] that the working pressure is the main factor affecting the droplet-size distribution of the sprinkler.

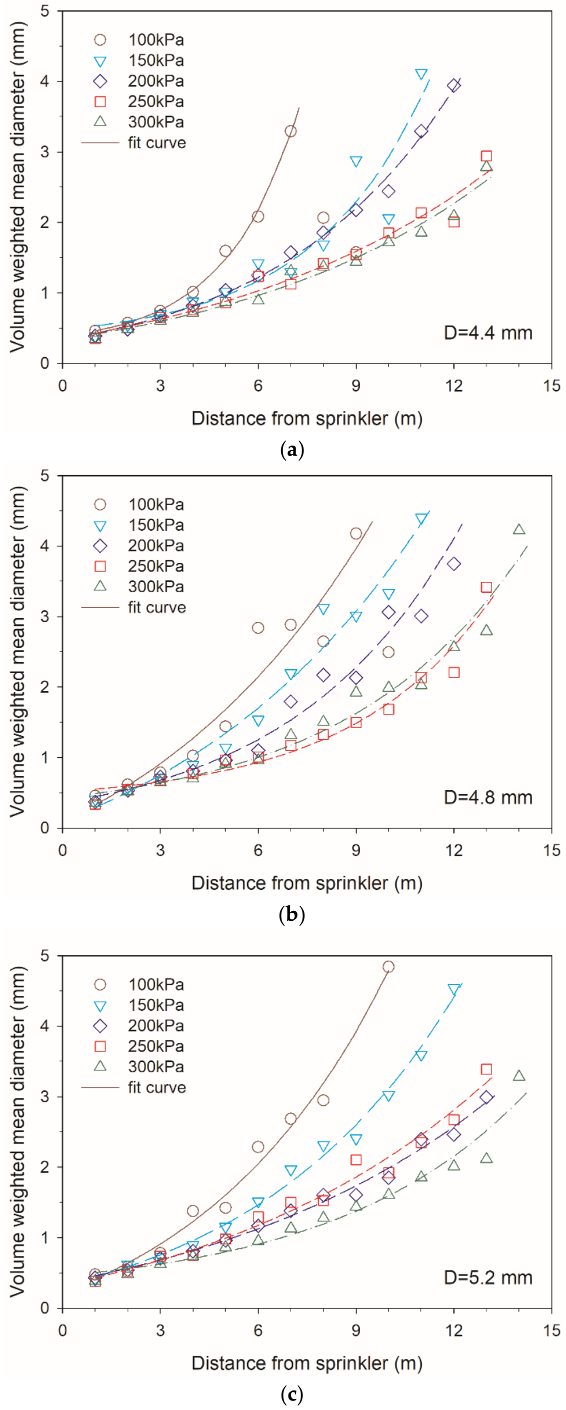


**Figure 7.** Droplets volume-weighted mean particle size (VMD) values versus distance from the sprinkler under different pressures. (**a**) D = 4.4 mm, (**b**) D = 4.8 mm, (**c**) D = 5.2 mm.

As seen in Figure 7, with an increase in the distance from the sprinkler, the droplet VMD values reached the maximum at the perimeter of the radius of throw. Under working pressures of 100, 150, 200, 250, and 300 kPa, the maximum VMD values for the nozzle size of 4.4 mm were 3.29, 4.12, 3.94, 2.94, and 2.79 mm, those for the nozzle size of 4.8 mm were 4.18, 4.41, 5.31, 3.42, and 4.22 mm, and those for the nozzle size of 5.2 mm were 5.96, 4.54, 2.99, 3.39, and 3.29 mm, respectively. It can be seen that the maximum VMD values increased initially and then decreased or decreased with the increase in working pressure. For most sprays, the formation process of water droplets was that (1) the water ejected from the nozzle and formed a jet, and then (2) through oscillation and air drag, the jet was finally broken into small water droplets. The droplet diameters were related to the thickness of the jet. Generally, the thicker the jet was, the larger the droplets were [36]. When the working pressure increased, the flow rate of the sprinkler increased, and the thickness of the jet also increased, resulting in an increase in the droplets' size. However, above a critical point, due to the effects of air drag and liquid surface tension, the coarse droplets broke up into fine droplets [14]. Therefore, when the working pressure increased to a critical point, the maximum VMD values of the sprinkler decreased. An independent sample *t*-test was used to test the significance in droplet VMD under different working pressures, nozzle sizes, and distances from the sprinkler.

The results indicate that the effects of the working pressure and distance from the sprinkler on droplet VMD were significant ($p < 0.01$), but the effect of the nozzle size on droplet VMD was not significant ($p = 0.147$). Considering the factors of the working pressure, distance to the sprinkler, and nozzle size on the influence of droplet VMD distribution, an empirical equation of VMD can be derived Equation (10).

$$d_V = 0.267 + 240.32D^{-0.416}P^{-1.198}e^{0.226x}\left(R^2 = 0.897\right) \quad (11)$$

where $d_V$ is the estimated VMD value in mm; $D$ is the nozzle diameter in mm; $P$ is the working pressure in kPa; $x$ is the distance from the sprinkler in m. The accuracy between the measured and calculated VMD values was evaluated by Equation (10). The value of RMSE is 0.351 and that of $R^2$ is 0.897 indicating a good agreement between observed and estimated VMD values.

The cumulative volume percentages of different droplet sizes at given distances from the sprinkler are presented in Figure 8 for different working conditions. The gradients of the cumulative volume were greater when the droplets were near the sprinkler, and the droplet size was small. However, the cumulative droplet volume distribution of the low-pressure sprinkler is different from conventional sprinklers, such as spray plate sprinklers and complete fluidic sprinklers. With an increase in the distance from the sprinkler, the cumulative droplet volume of fine droplets ($d < 1$ mm) decreased initially and then increased. For example, under the operating pressure of 200 kPa and distances from the nozzle of 2, 4, 6, 8, 10, and 12 m, the cumulative volume percentages of fine droplets ($d \leq 1$ mm) with the nozzle size of 4.4 mm were 100%, 96.16%, 83.86%, 72.27%, 81.69%, and 94.57%, respectively, those of fine droplets with the nozzle size of 4.8 mm were 100%, 97.14%, 85.60%, 82.47%, 85.95%, and 94.66%, respectively, and those with the nozzle size of 5.2 mm were 99.99%, 97.12%, 83.75%, 84.83%, 84.60%, and 98.06%, respectively. These results differ from those of other studies, which found that the cumulative volume percentages of fine droplets decreased with an increase in distance from the sprinkler [14,19]. This may be attributed to the differences in the structure and functioning principle of the sprinkler. The low-pressure sprinkler has a diffuser in front of the plate, which can promote the breakup of the jet and change the droplet size distribution pattern. However, for spray plate sprinklers and complete fluidic sprinklers, jets break up into fine spray due to dominant forces, such as drag and surface tension, that influence droplet size [14]. Additionally, the droplets deposited at each observed distance were not of the same diameter but varied (Figure 8), implying that the process of droplet formation and breakup is continuous along the jet.

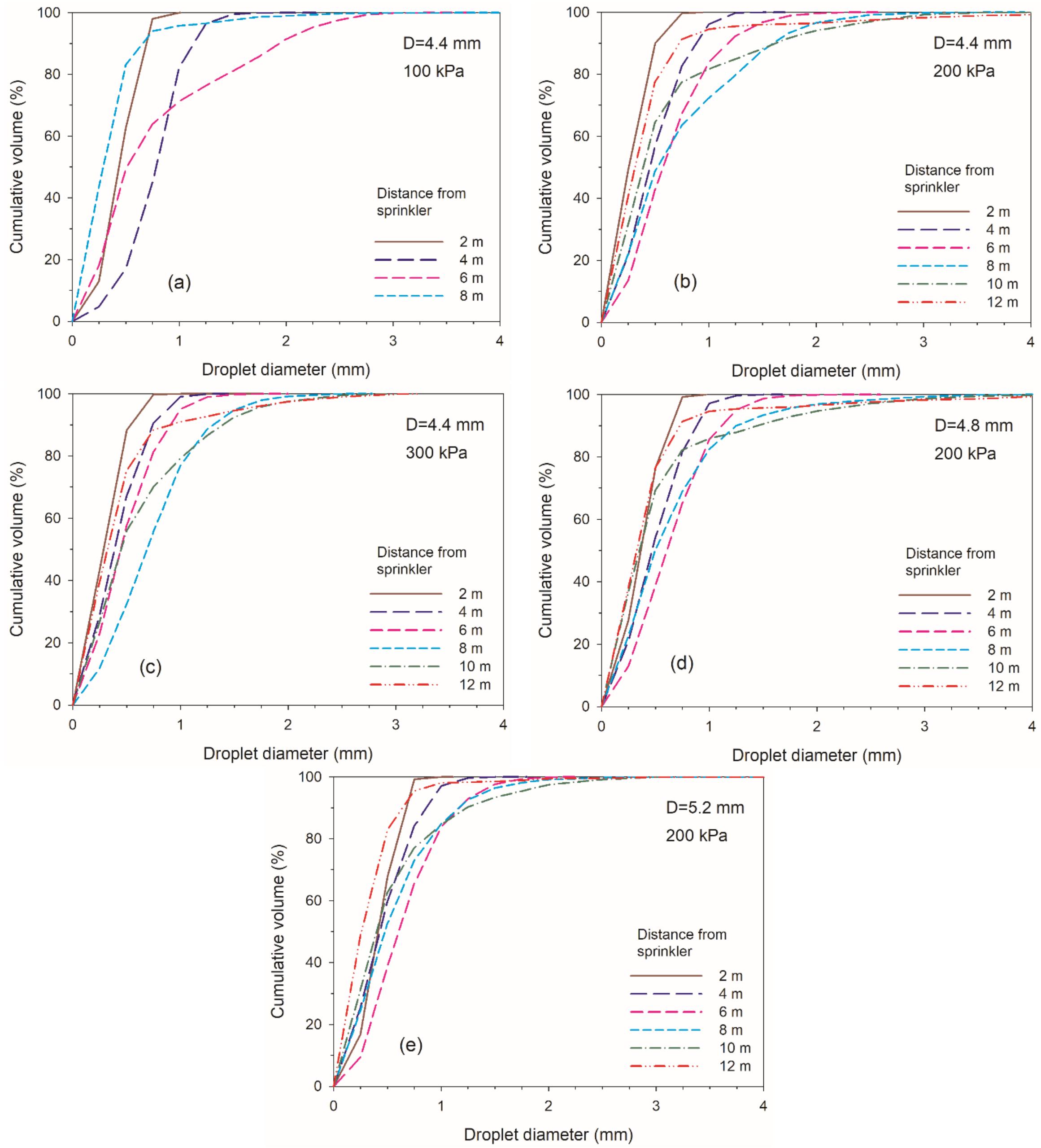


**Figure 8.** Droplet cumulative volume of the sprinklers with the nozzle size of 4.4 mm under the working pressures of (**a**) 100 kPa, (**b**) 200 kPa, (**c**) 300 kPa, and nozzle sizes of (**d**) 4.8 mm and (**e**) 5.2 mm under the working pressure of 200 kPa.

## *3.4. Droplet Velocity*

Droplet velocity is one of the important characteristic indexes that influence the droplet kinetic energy. Figure 9 represents the relationship between droplet mean velocity and the droplet diameter of the sprinkler with the nozzle size of 4.8 mm under three different working pressures. It can be seen that the droplet mean velocities increased as droplet diameters increased under different working conditions. An independent sample *t*-test was used to test the significance in droplet mean velocity under different droplet diameters and distances from the sprinkler. The results indicate that the effect of the droplet size on droplet mean velocity was significant ($p < 0.01$), but the effect of the distance from the sprinkler on droplet mean velocity was not significant ($p$ = 0.143). In previous studies [14,30], a logarithmic relation was derived between droplet diameter and mean droplet velocity Equation (12).

$$\overline{v}_d = a\ln(d) + b \tag{12}$$

where $\bar{v}_d$ is the mean velocity of a droplet of $d$ mm in diameter in m s$^{-1}$; $a$ and $b$ are coefficients. The coefficients were obtained using regression analysis for each nozzle size and working pressure combination.

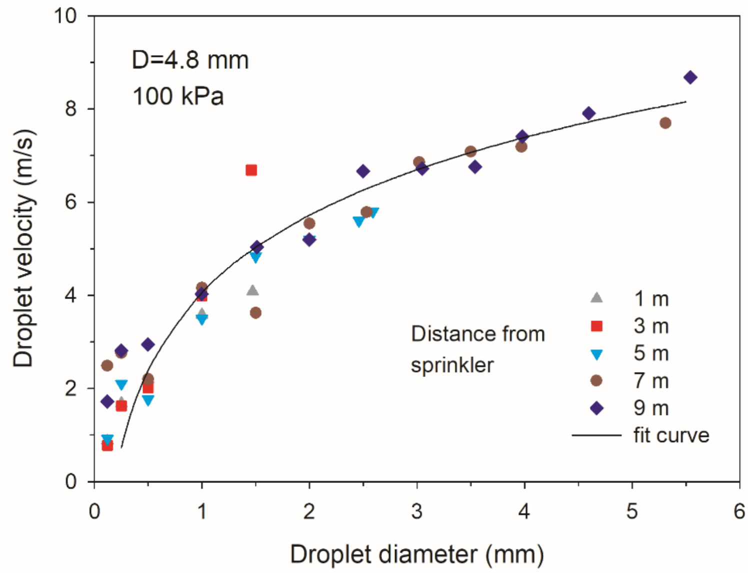


(**a**)

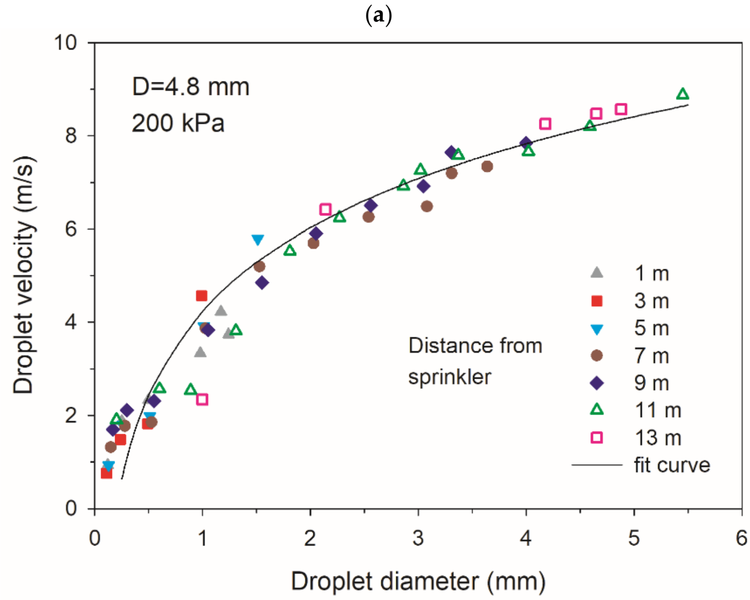


(**b**)

**Figure 9.** *Cont.*

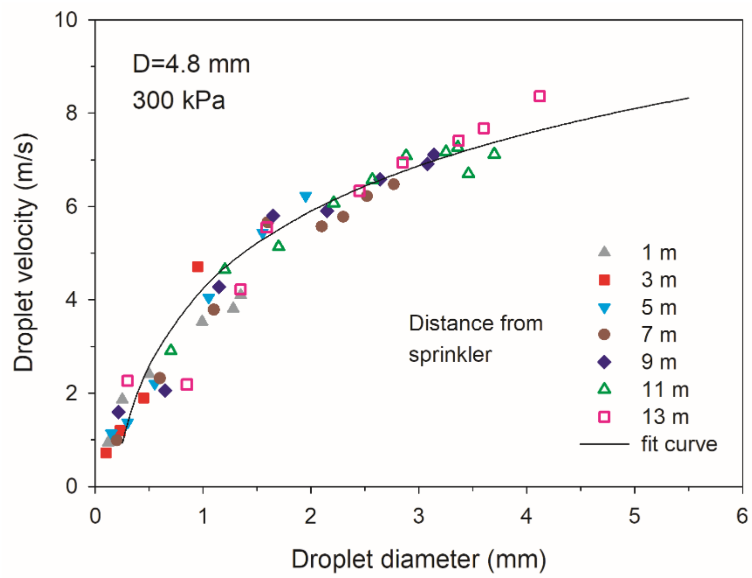


(**c**)

**Figure 9.** Relationships between droplet mean velocity and droplet diameter of the sprinkler with a nozzle size of 4.8 mm under different working pressures. (**a**) P = 100 kPa, (**b**) P = 200 kPa, (**c**) P = 300 kPa.

The logarithmic relationships between droplet mean velocity and diameter are shown in Table 2. The $R^2$ values are greater than 0.837 in all cases, indicating a good overall fit between droplet velocity and diameter.

**Table 2.** Logarithmic relationships between droplet mean velocity and diameter under different working pressures and their $R^2$ values.

| Nozzle Size (mm) | Working Pressure (kPa) | Relational Expression | $R^2$ |
|---|---|---|---|
| 4.4 | 100 | $\overline{v}_d = 2.115 \ln d + 4.102$ | 0.934 |
| | 200 | $\overline{v}_d = 2.541 \ln d + 4.203$ | 0.950 |
| | 300 | $\overline{v}_d = 3.119 \ln d + 4.499$ | 0.837 |
| 4.8 | 100 | $\overline{v}_d = 2.403 \ln d + 4.057$ | 0.969 |
| | 200 | $\overline{v}_d = 2.597 \ln d + 4.232$ | 0.963 |
| | 300 | $\overline{v}_d = 2.394 \ln d + 4.244$ | 0.965 |
| 5.2 | 100 | $\overline{v}_d = 2.350 \ln d + 4.171$ | 0.920 |
| | 200 | $\overline{v}_d = 3.287 \ln d + 4.480$ | 0.902 |
| | 300 | $\overline{v}_d = 2.714 \ln d + 4.555$ | 0.928 |

As seen in Figure 9 and Table 2, at a given droplet diameter, the mean droplet velocity increased with an increase in the working pressure. Taking the nozzle size of 5.2 mm as an example, the mean velocities of a droplet of 1 mm in diameter under operating pressures of 100, 200, and 300 kPa were 3.62, 3.77, and 3.85 m $s^{-1}$, those of a droplet with a diameter of 2 mm were 5.66, 6.08, and 6.58 m $s^{-1}$, and those of a droplet with a diameter of 3 mm were 6.89, 7.53, and 7.74 m $s^{-1}$, respectively. The effect of the working pressure on droplet velocity can be attributed to the flow rate of the sprinkler increasing with the increasing working pressure. The flow rate ($Q$, $m^3$ $s^{-1}$) is equal to the velocity of the jet ($v$, m $s^{-1}$) multiplied by the cross-sectional area of the nozzle ($A$, $m^2$; $Q = Av$). As a given nozzle size, the velocity of the jet increases with the increasing flow rate. Therefore, the velocity of the droplet increased with an increase in the working pressure. The result of the significance test showed that the effect of nozzle size on droplet velocity was not significant ($p = 0.319$).

Considering the influence of the factors of working pressure and nozzle size on mean droplet velocity, an empirical equation of droplet mean velocity can be derived Equation (13).

$$\overline{v}_d = 4.287 + 0.259D^{0.636}P^{0.252}\ln d\left(R^2 = 0.905\right) \quad (13)$$

where $\bar{v}_d$ is the mean velocity of a droplet of $d$ mm in diameter in m s$^{-1}$; $D$ is the nozzle diameter in mm; $P$ is the working pressure in kPa.

### 3.5. Droplet Angle

The mean values of the droplet angle versus the distance from the sprinkler are shown in Figure 10. Contrary to the results for droplet diameter and velocity, the mean trajectory angle of the droplets decreased with an increase in the distance from the sprinkler. Meanwhile, the mean trajectory angle of the droplets at the same distance from the sprinkler increased with increasing operating pressures. It can be attributed to the wetted radius increased with an increase in working pressure. Taking the nozzle size of 4.8 mm as an example, under the working pressures of 100, 200, and 300 kPa, the mean droplet angles at a distance from the sprinkler of 3 m were 84.24°, 84.75°, and 85.82°, those at a distance from the sprinkler of 6 m were 54.76°, 77.82°, and 84.30°, and those at a distance from the sprinkler of 10 m were 55.83°, 58.44°, and 64.73°, respectively. Due to the same elevation angle of the sprinkler plate for the three nozzles, the result of the significance test showed that the effect of nozzle size on the mean droplet angle was not significant ($p$ = 0.734).

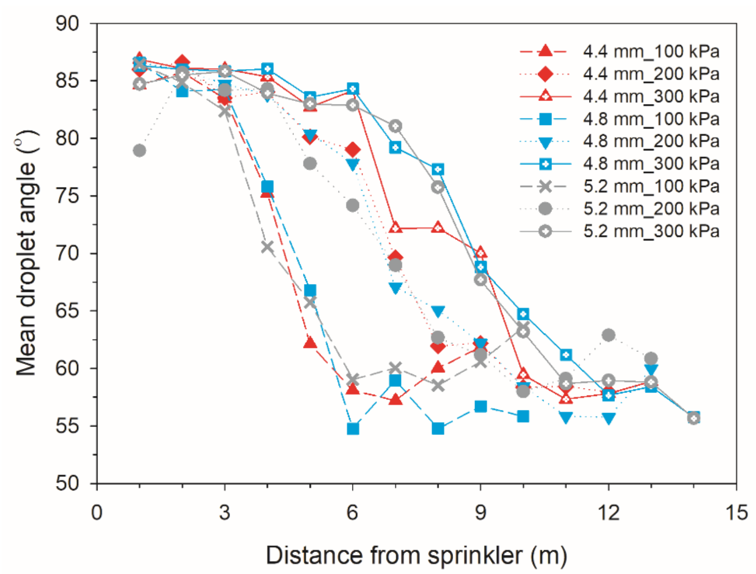


**Figure 10.** Mean droplet trajectory angle versus distance from the sprinkler for three nozzle sizes under different working pressure.

### 3.6. Kinetic Energy

The kinetic energy per unit droplet volume ($KE_{di}$) values at different distances from the sprinkler are presented in Figure 11. The $KE_{di}$ value near the sprinkler was low in all cases and increased with an increase in the distance from the sprinkler. The analysis of variance showed that working pressure had a significant effect on the $KE_{di}$ ($p < 0.01$). At the same radial location, the $KE_{di}$ decreased with increasing working pressure, which was similar to the effect of the working pressure on the droplet size. In addition, under the low working pressures of 100 and 150 kPa, the maximum $KE_{di}$ value increased with an increase in nozzle size. Under the lowest working pressure of 100 kPa, the maximum $KE_{di}$ values with nozzle sizes of 4.4, 4.8, and 5.2 mm were 22.24, 27.92, and 33.97 J L$^{-1}$, and they were 29.69, 30.54, and 32.23 J L$^{-1}$ under the working pressure of 150 kPa. Considering the influence of the factors of working pressure, nozzle size, and distance from the sprinkler on $KE_{di}$, Equation (14) gives an empirical equation for $KE_{di}$.

$$KE_{di} = 16.553D^{0.077}P^{-0.394}i - 2.529\left(R^2 = 0.896\right) \tag{14}$$

where $D$ is the nozzle diameter in mm; $P$ is the working pressure in kPa; $i$ is the distance from the sprinkler in m.

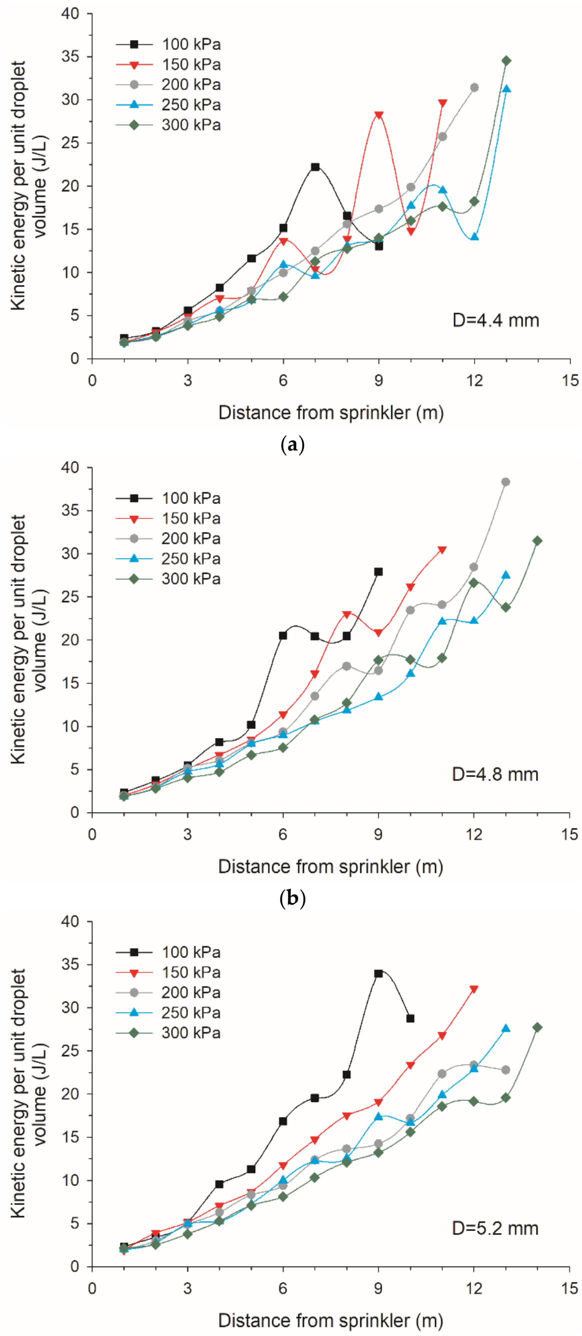


(**a**) (**b**) (**c**)

**Figure 11.** Per unit droplet volume kinetic energy distribution in different distances from the sprinkler. (**a**) D = 4.4 mm, (**b**) D = 4.8 mm, (**c**) D = 5.2 mm.

Specific power represents the rate at which kinetic energy is transferred to the soil surface; it is also referred to as droplet energy flux [37]. The radial SP of the low-pressure sprinkler was calculated based on the droplet diameter, droplet velocity, and water application rate at each sampling point (Figure 12). Under the low pressures of 100 and 150 kPa, along the wetted radius, the computed SP value increased and then decreased, with a peak value at a certain distance. When the working pressure increased from 100 to 300 kPa, the peak value of SP decreased, and the radial SP distribution of the sprinkler became more uniform. Under the working pressures of 100, 150, 200, 250, and 300 kPa, the peak SP values with the nozzle size of 4.4 mm reached 0.023, 0.033, 0.018, 0.012, and 0.013 W m$^{-2}$, those with the nozzle size of 4.8 mm were 0.038, 0.036, 0.018, 0.015, and 0.017 W m$^{-2}$, and those with the nozzle size of 5.2 mm were 0.091, 0.029, 0.022, 0.019, and 0.017 W m$^{-2}$, respectively. The peak value of SP increased with an increase in the nozzle size under the same working pressure. Since the SP value depended on the water application rate, the effects of working pressure and nozzle size on SP were similar to those of pressure and nozzle size on the application rate. The maximum SP value was observed for the sprinkler with the largest nozzle size under the lowest working pressure in all cases, as illustrated in Figure 12.

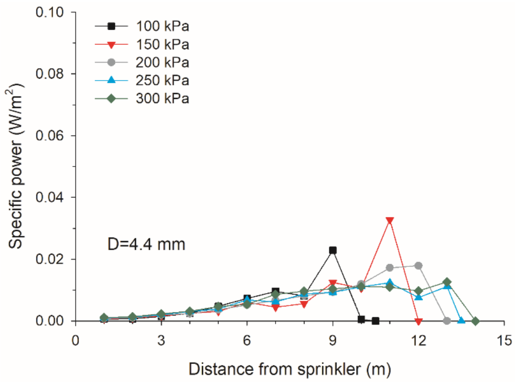


(**a**)

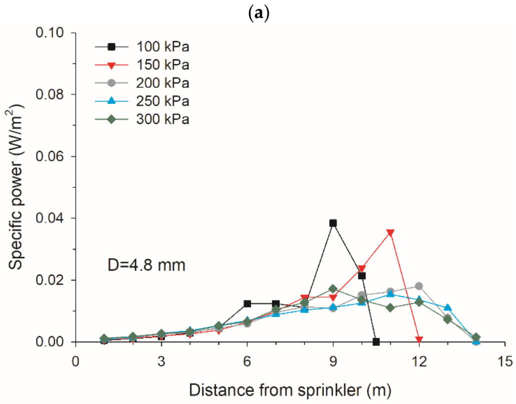


(**b**)

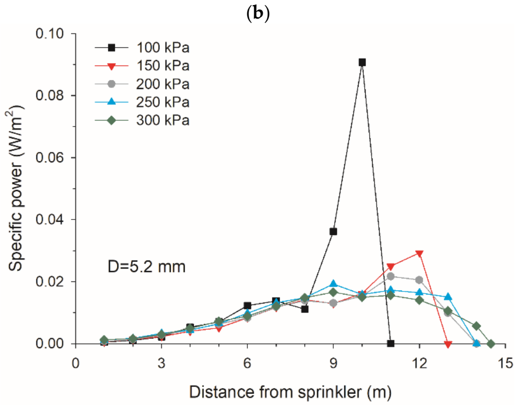


(**c**)

**Figure 12.** Radial distribution of specific power under different working pressures. (**a**) D = 4.4 mm, (**b**) D = 4.8 mm, (**c**) D = 5.2 mm.

As seen in Figure 12, when the distance from the sprinkler was less than 6 m, the SP was less than 0.012 W m$^{-2}$; this is due to the low droplet velocity and small droplet size near the sprinkler. The peak values and distances of peak points of SP and application rate from the sprinkler are shown in Table 3. It can be seen that the peak points of application rate and SP for the low-pressure sprinkler were almost overlapping. Although the size and velocity of water droplets reached their maximum values at the outer end, the peak value of SP was not at the outermost end of the wetted radius, and the rapid decrease in sprinkler application rate led to the decrease in SP. Furthermore, although the droplet velocity was lower under the lowest operating pressure of 100 kPa, the high application rate of the sprinkler led to a high SP value. Therefore, the SP peak occurs only when the droplet size, velocity, and application rate are maintained at a high level. The high kinetic energy of spray water results in a soil surface seal, which often reduces the infiltration rate and promotes runoff, resulting in soil erosion and a waste of water resources.

**Table 3.** Distances of peak points and peak values of specific power and application rate from the sprinkler.

| Nozzle Size (mm) | Pressure (kPa) | $AR_m$_i (m) | $SP_m$_i (m) | $AR_m$ (mm h$^{-1}$) | $SP_m$ (W m$^{-2}$) |
|---|---|---|---|---|---|
| 4.4 | 100 | 9.5 | 9 | 8.507 | 0.023 |
| | 150 | 11 | 11 | 3.975 | 0.033 |
| | 200 | 10.5 | 12 | 2.410 | 0.018 |
| | 250 | 10.5 | 11 | 2.432 | 0.012 |
| | 300 | 7 | 13 | 2.735 | 0.013 |
| 4.8 | 100 | 9.5 | 9 | 7.280 | 0.038 |
| | 150 | 11 | 11 | 4.190 | 0.036 |
| | 200 | 10.5 | 12 | 2.450 | 0.018 |
| | 250 | 8 | 11 | 3.125 | 0.015 |
| | 300 | 8 | 9 | 3.605 | 0.017 |
| 5.2 | 100 | 10 | 10 | 11.354 | 0.091 |
| | 150 | 11.5 | 12 | 3.720 | 0.029 |
| | 200 | 8 | 11 | 3.672 | 0.022 |
| | 250 | 8 | 9 | 4.224 | 0.019 |
| | 300 | 9 | 9 | 4.525 | 0.017 |

Note: $AR_m$_i is the distance of the peak point of the application rate from the sprinkler. $SP_m$_i is the distance of the peak point of specific power from the sprinkler. $AR_m$ is the peak value of the application rate. $SP_m$ is the peak value of specific power.

## 4. Discussion

Operating pressure has been reported to be a significant influence on water distribution [8], while its influence on kinetic energy distribution has been rarely mentioned [26], especially for low-pressure sprinklers. Due to the low breakup degree of the jet flow under low working pressure, the specific power and application rate under 100 kPa were significantly higher than those under other working pressures (Figures 6 and 12). It is easy to lead a lower infiltration rate and increase the formation of surface seal and runoff [34]. Meanwhile, the specific power increased with increasing nozzle size. Therefore, it is not recommended to equip the sprinkler with a large nozzle under low working pressure.

The droplet size and kinetic energy per unit droplet volume increased with the increase in distance from the sprinkler and reached a maximum at the edge of the wetted area [Figures 7 and 11]. In the design of sprinkler, low specific power and uniform kinetic energy distribution can be obtained if the water application rate can be decreased along the radial direction.

When designing an irrigation system, often the application rate is the factor that designers consider above all others in selecting a sprinkler unit because the aim of irrigation is to satisfy the water requirements of the crop and maintain crop yield [10,34]. Since the low-pressure sprinkler is not recommended to equip with a large nozzle, the flow rate and average water application rate of the sprinkler are lower. For crops with higher water requirements, using low-pressure sprinklers means longer irrigation time is needed. The benefits associated with lower working pressure may be negated by the longer working time. Therefore, low-pressure sprinkler irrigation may be more applicable for crops with lower water requirements and for irrigation on sensitive crops and soils. This study could enable designers to properly analyze the water distribution patterns, drift, and evaporation losses and the kinetic energy of droplets produced by the sprinkler, and the results may be helpful in the better use of water by low-pressure sprinklers. The effects of the kinetic energy of low-pressure rotating sprinklers on soil water dynamics should be further investigated.

## 5. Conclusions

The spray characteristics of a low-pressure rotating sprinkler were evaluated in this study. The droplet characteristics were measured using a 2DVD, and the kinetic energy was calculated based on the experimental data. The results were as follows.

(a) The relations among mean droplet diameter, working pressure, sprinkler nozzle, and distance from sprinkler were indicated by the droplet diameter model in this paper. The relationships between the droplet velocity and droplet diameter were described by a logarithmic function model. The correlation coefficients of these models reached as high as 0.9 under different working pressures and nozzle sizes.
(b) An empirical equation was developed to estimate the kinetic energy per unit droplet volume at different distances from the sprinkler as functions of the working pressure and nozzle size. With an increase in working pressure, the peak specific power and application rate decreased while the rotation speed and droplet trajectory angle increased.
(c) The working pressure of the sprinkler should not be below 150 kPa since the quality of the water application decreased under the lowest working pressure of 100 kPa. It is necessary to select the nozzles adapted to the working pressure of the sprinkler irrigation system.

**Author Contributions:** Investigation, R.C. and X.G.; resources, H.L. and J.W.; data curation, R.C.; writing—original draft preparation, R.C.; writing—review and editing, R.C.; and funding acquisitions, H.L. and J.W. and R.C. All authors have read and agreed to the published version of the manuscript.

**Funding:** This study was financially supported by the National Natural Science Foundation of China (Grant numbers 51939005, 51679109, 51709130), the China Postdoctoral Science Foundation-funded project (Grant number 2017M621653), and the Postgraduate Scientific Research and Innovation Plan of Jiangsu Province (Grant number KYCX20_3019). And National key Research and Development Project of China (Grant number 2017YFD0201502).

**Conflicts of Interest:** The authors declare no conflict of interest.

## References

1. Tal, A. Rethinking the sustainability of Israel's irrigation practices in the drylands. *Water Res.* **2016**, *90*, 387–394. [CrossRef] [PubMed]
2. UNESCO. *The United Nations World Water Development Report 2014: Water and Energy*; The United Nations world water development report; UNESCO Pub.: Paris, France, 2014.
3. Zhou, B.; Li, Y.K.; Xue, S.; Feng, J. Variation of microorganisms in drip irrigation systems using high-sand surface water. *Agric. Water Manag.* **2019**, *218*, 37–47. [CrossRef]
4. Lal, R. Carbon emission from farm operations. *Environ. Int.* **2004**, *30*, 981–990. [CrossRef] [PubMed]
5. Wang, J.; Chen, R. An improved finite element model for the hydraulic analysis of drip irrigation subunits considering local emitter head loss. *Irrig. Sci.* **2020**, *38*, 147–162. [CrossRef]
6. Zapata, N.; Robles, O.; Playán, E.; Paniagua, P.; Romano, C.; Salvador, R.; Montoya, F. Low-pressure sprinkler irrigation in maize: Differences in water distribution above and below the crop canopy. *Agric. Water Manag.* **2018**, *203*, 353–365. [CrossRef]

7. Moreno, M.A.; Ortega, J.F.; Córcoles, J.I.; Martínez, A.; Tarjuelo, J.M. Energy analysis of irrigation delivery systems: Monitoring and evaluation of proposed measures for improving energy efficiency. *Irrig. Sci.* **2010**, *28*, 445–460. [CrossRef]
8. Zhang, L.; Merkley, G.P.; Pinthong, K. Assessing whole-field sprinkler irrigation application uniformity. *Irrig. Sci.* **2013**, *31*, 87–105. [CrossRef]
9. Dieter, C.A.; Maupin, M.A.; Caldwell, R.R.; Harris, M.A.; Ivahnenko, T.I.; Lovelace, J.K.; Barber, N.L.; Linsey, K.S. Estimated use of water in the United States in 2015. *US Geol. Surv. Circ.* **2018**, *1441*, 36.
10. Robles, O.; Playán, E.; Cavero, J.; Zapata, N. Assessing low-pressure solid-set sprinkler irrigation in maize. *Agric. Water Manag.* **2017**, *191*, 37–49. [CrossRef]
11. Cai, Y.H.; Wu, P.T.; Zhang, L.; Zhu, D.L.; Wu, S.J.; Zhao, X.; Dong, Z. Prediction of flow characteristics and risk assessment of deep percolation by ceramic emitters in loam. *J. Hydrol.* **2018**, *566*, 901–909. [CrossRef]
12. Jiménez-Bello, M.A.; Royuela, A.; Manzano, J.; Prats, A. García; Martínez-Alzamora, F. Methodology to improve water and energy use by proper irrigation scheduling in pressurised networks. *Agric. Water Manag.* **2015**, *149*, 91–101. [CrossRef]
13. Martínez, J.M.; Martínez, R.S.; Martínbenito, J.M.T. Analysis of water application cost with permanent set sprinkler irrigation systems. *Irrig. Sci.* **2004**, *23*, 103–110. [CrossRef]
14. Sayyadi, H.; Nazemi, A.H.; Sadraddini, A.A.; Delirhasannia, R. Characterising droplets and precipitation profiles of a fixed spray-plate sprinkler. *Biosyst. Eng.* **2014**, *119*, 13–24. [CrossRef]
15. Robles-Rovelo, C.O.; Ruiz, N.Z.; Tolosa, J.B.; Félix-Félix, J.R.; Latorre, B. Characterization and Simulation of a Low-Pressure Rotator Spray Plate Sprinkler Used in Center Pivot Irrigation Systems. *Water* **2019**, *11*, 1684. [CrossRef]
16. Li, Y.C.; Hui, X.; Yan, H.J.; Chen, D.Y. Effects of Travel Speed and Collector on Evaluation of the Water Application Uniformity of a Center Pivot Irrigation System. *Water* **2020**, *12*, 1916. [CrossRef]
17. Zhang, L.; Fu, B.Y.; Ren, N.W.; Huang, Y. Effect of pulsating pressure on water distribution and application uniformity for sprinkler irrigation on sloping land. *Water* **2019**, *11*, 913. [CrossRef]
18. Kincaid, D.C. Spray drop kinetic energy from irrigation sprinklers. *Trans. ASAE* **1996**, *39*, 847–853. [CrossRef]
19. Liu, J.P.; Liu, X.F.; Zhu, X.Y.; Yuan, S.Q. Droplet characterisation of a complete fluidic sprinkler with different nozzle dimensions. *Biosyst. Eng.* **2016**, *148*, 90–100. [CrossRef]
20. Lima, J.L.M.P.D.; Torfs, P.J.J.F.; Singh, V.P. A mathematical model for evaluating the effect of wind on downward-spraying rainfall simulators. *CATENA* **2002**, *46*, 221–241. [CrossRef]
21. Yan, H.J.; Bai, G.; He, J.Q.; Lin, G. Influence of droplet kinetic energy flux density from fixed spray-plate sprinklers on soil infiltration, runoff and sediment yield. *Biosyst. Eng.* **2011**, *110*, 213–221. [CrossRef]
22. Young, R.A.; Wiersma, J.L. The role of rainfall impact in soil detachment and transport. *Water Resour. Res.* **1973**, *9*, 1629–1636. [CrossRef]
23. Angulo Martínez, M.; Barros, A.P. Measurement uncertainty in rainfall kinetic energy and intensity relationships for soil erosion studies: An evaluation using PARSIVEL disdrometers in the Southern Appalachian Mountains. *Geomorphology* **2015**, *228*, 28–40. [CrossRef]
24. Thompson, A.L.; Gilley, J.R.; Norman, J.M. A sprinkler water droplet evaporation and plant canopy model: 2. Model application. *Trans. ASAE* **1993**, *36*, 743–750. [CrossRef]
25. Schneider, A.D. Efficiency and uniformity of the LEPA and spray sprinkler methods: A review. *Trans. ASAE* **2000**, *43*, 937–944. [CrossRef]
26. Ge, M.S.; Wu, P.T.; Zhu, D.L.; Zhang, L. Analysis of kinetic energy distribution of big gun sprinkler applied to continuous moving hose-drawn traveler. *Agric. Water Manag.* **2018**, *201*, 118–132. [CrossRef]
27. ISO 15886-3. *Agricultural Irrigation Equipment—Sprinklers—Part 3: Characterization of Distribution and Test Methods*; ISO: Geneva, Switzerland, 2016.
28. ASAE Standards. *Procedure for Sprinkler Testing and Performance Reporting*; ASAE S398.1.; ASABE: St Joseph, MI, USA, 1985.
29. Playán, E.; Salvador, R.; Faci, J.M. Day and night wind drift and evaporation losses in sprinkler solid-sets and moving laterals. *Agric. Water Manag.* **2005**, *76*, 139–159. [CrossRef]
30. Seginer, I. Water distribution from medium pressure sprinklers. *J. Irrig. Drain. E-ASCE* **1963**, *89*, 13–30.
31. King, B.A.; Bjorneberg, D.L. Characterizing droplet kinetic energy applied by moving spray-plate center-pivot irrigation sprinklers. *Trans. ASABE* **2010**, *53*, 137–145. [CrossRef]

32. King, B.A. Moving spray-plate center-pivot sprinkler rating index for assessing runoff potential. *Trans. ASABE* **2016**, *59*, 225–237.
33. Liu, J.P.; Zhu, X.Y.; Yuan, S.Q.; Wan, J.H.; Chikangaise, P. Hydraulic performance assessment of sprinkler irrigation with rotating spray plate sprinklers in indoor experiments. *J. Irrig. Drain. E-ASCE* **2018**, *144*, 06018005. [CrossRef]
34. Ge, M.S.; Wu, P.T.; Zhu, D.L.; Zhang, L. Comparisons of spray characteristics between vertical impact and turbine drive sprinklers—A case study of the 50PYC and HY50 big gun-type sprinklers. *Agric. Water Manag.* **2020**, *228*, 105847. [CrossRef]
35. Montero, J.; Tarjuelo, J.M.; Carrión, P. Sprinkler droplet size distribution measured with an optical spectropluviometer. *Irrig. Sci.* **2003**, *22*, 47–56. [CrossRef]
36. Ashgriz, N.; Li, X.; Sarchami, A. Instability of liquid sheets. In *Handbook of Atomization and Sprays*; Ashgriz, N., Ed.; Springer: New York, NY, USA, 2011; pp. 75–95.
37. Thompson, A.L.; James, L.G. Water droplet impact and its effect on infiltration. *Trans. ASAE* **1985**, *28*, 1506–1510. [CrossRef]

**Publisher's Note:** MDPI stays neutral with regard to jurisdictional claims in published maps and institutional affiliations.